Characterizing tropical overshooting deep convection from joint analysis of CloudSat and geostationary satellite observations

Hanii Takahashi[1,2] and Zhengzhao Johnny Luo[3]

Received 30 September 2013; revised 27 November 2013; accepted 1 December 2013; published 8 January 2014.

[1] Tropical overshooting deep convection (ODC) plays an important role in affecting the heat and constituent budgets of the upper troposphere and lower stratosphere. This study investigates the properties and behaviors of such intense deep convection using a combination of CloudSat observations and geostationary satellite data. Our study approaches the subject from two unique perspectives: first, W-band cloud profiling radar (CPR) observations from CloudSat are used, which add to our knowledge of the internal vertical structure of tropical ODC; second, each snapshot observation from CloudSat is cast into the time evolution of the convective systems through joint analysis of geostationary satellite data, which provides a lifecycle view of tropical ODC. Climatology of tropical ODC based on CloudSat data is first presented and compared with previous works. Various parameters from CloudSat observations pertaining to cloud vertical extent, convective intensity, and convective environment are analyzed. Although results broadly agree with previous studies, we show that CloudSat CPR is capable of capturing both small cloud particles and large precipitation-size particles, thus presenting a more complete depiction of the internal vertical structure of tropical ODC. Geostationary satellite observations are analyzed in conjunction with CloudSat data to identify the life stage of the convective systems (CSs) in which ODC is embedded. ODC associated with the growing, mature, and dissipating stage of the CSs represents, respectively, 66.2%, 33.4%, and 0.4% of the total population. Convective intensity of the ODC is found to be stronger during the growing stage than the mature stage.

Citation: Takahashi, H., and Z. J. Luo (2014), Characterizing tropical overshooting deep convection from joint analysis of CloudSat and geostationary satellite observations, *J. Geophys. Res. Atmos.*, *119*, 112–121, doi:10.1002/2013JD020972.

1. Introduction

[2] It has been well established that tropical deep convective clouds are an important agent in transporting energy and moisture (and other trace gasses) from the planetary boundary layer to the upper troposphere [e.g., *Riehl and Malkus*, 1958; *Sun and Lindzen*, 1993; *Soden and Fu*, 1995; *Jiang et al.*, 2004; *Su et al.*, 2006; *Jiang et al.*, 2007]. Of special interest is a small subset of deep convection that is strong enough to overshoot the corresponding level of neutral buoyancy (LNB). Tropical overshooting deep convection (ODC) has the potential of penetrating into the tropical tropopause layer (TTL) or even directly into the lower stratosphere (This paper contains many abbreviations and acronyms. To facilitate reading, we compile them all in Table 1). Considerable debates have been seen in the literature concerning the exact role played by tropical ODC in affecting the lower stratospheric heat and moisture [e.g., *Sherwood and Dessler*, 2000; *Küpper et al.*, 2004; *Kuang and Bretherton*, 2004]. One particularly uncertain area is the following: At what height level and at what rate does deep convective mass affect the TTL and lower stratosphere [*Fueglistaler et al.*, 2009]? On the one hand, since tropical ODC is a less frequently occurring phenomenon [e.g., *Luo et al.*, 2008], its importance in transporting mass and constituents could be overshadowed by slow but ubiquitously occurring ascent in TTL, as shown in *Küpper et al.* [2004]. But on the other hand, these small numbers of ODC events produce disproportionately profound effects on the thermodynamics and chemical compositions of the TTL and lower stratosphere [*Kuang and Bretherton*, 2004]. Moreover, tropical ODC plays a critical role in transporting short-lived chemical compounds from near the surface to the lower stratosphere, which is hard to achieve by slow ascent [e.g., *Shepherd*, 2008; *Bergman et al.*, 2012].

[3] Understanding these important influences requires, in part, ways of observing the tropics-wide distribution of ODC as well as their properties and behaviors. A number of satellite-based studies have been conducted in the past. Using IR brightness temperature (TB) measurements, *Gettelman et al.* [2002] described the global distributions of tropical deep

[1]Program in Earth and Environmental Sciences, Graduate Center, CUNY, New York, New York, USA.
[2]Now at Jet Propulsion Laboratory, California Institute of Technology, Pasadena, California, USA.
[3]Department of Earth and Atmospheric Sciences and CREST Institute, City College of New York, CUNY, New York, New York, USA.

Corresponding author: Z. J. Luo, Department of Earth and Atmospheric Sciences and CREST Institute, City College of New York, CUNY, New York, NY 10031, USA. (luo@sci.ccny.cuny.edu)

2169-897X/14/10.1002/2013JD020972

Table 1. List of Abbreviations and Acronyms and Their Meanings

Acronyms	Meanings
CALIPSO	Cloud-Aerosol Lidar and Infrared Pathfinder Satellite Observation
CAPE	Convective available potential energy
CBH	Cloud-based height
CC	Convective Clusters
CPR	Cloud-profiling radar
CS	Convective system
CT	Convection Tracking
CTETD	Cloud top-echo top distance
CTH	Cloud top height
DC	Deep convection
ECMWF	European Centre for Medium-Range Weather Forecasts
EP	Eastern Pacific
ETH	Echo top height
IR	Infrared radiation
ISCCP	International Satellite Cloud Climatology Project
ITCZ	Intertropical Convergence Zone
LNB	Level of neutral buoyancy
MODIS	Moderate Resolution Imaging Spectroradiometer
ODC	Overshooting deep convection
OSD	Overshooting distance
PBL	Planetary boundary layer
PR	Precipitation Radar
R	Radius size
TB	Brightness temperature
TRMM	Tropical Rain Measuring Mission
TTL	Tropical tropopause layer
TWP	Tropical warm pool

convection that penetrates into the lower stratosphere. *Bedka et al*. [2010, 2012] specifically examined the overshooting tops with TB lower than the surrounding anvil clouds by some thresholds. *Rossow and Pearl* [2007] took a different approach by characterizing the nature of the convective systems that contain cold pixels representing overshoots into the stratosphere; it was found that most of them are larger, organized convective systems. *Hong et al*. [2005] utilized high-frequency passive microwave measurements (~183 GHz) to identify tropical ODC based on the scattering effect in the microwave due to large ice particles lofted by strong convective motion. *Liu and Zipser* [2005] and *Liu et al*. [2007] examined the vertical structure and intensity of penetrative deep convection using data from the Tropical Rain Measuring Mission (TRMM) Precipitation Radar (PR) operating at 13.8 GHz that is sensitive to moderate to heavy precipitation.

[4] Launch of CloudSat in 2006, which carries with it a 94 GHz cloud-profiling radar sensitive to both cloud- and precipitation-size particles, provides another opportunity to study tropical ODC. *Luo et al*. [2008] used a combination of CloudSat radar reflectivity profiles and MODIS (Moderate Resolution Imaging Spectrometer) IR brightness temperatures to infer life cycle of tropical penetrating deep convection. *Chung et al*. [2008] also used CloudSat radar data and collocated IR information (from Meteosat-8) to study the relation between warm water vapor pixels and high-reaching tropical deep convection. *Iwasaki et al*. [2010, 2012] analyzed CloudSat, CALIPSO (Cloud-Aerosol Lidar and Infrared Pathfinder Satellite Observation), and MODIS to study the mixing of overshoots with the stratospheric air. This paper builds upon these previous works and further studies tropical ODC using CloudSat data. An important aspect of this current study is the combination of CloudSat and geostationary satellite observations, the latter being obtained from the International Satellite Cloud Climatology Project (ISCCP) Convection Tracking (CT) database. Recent publications by *Luo et al*. [2009, 2010] have shown that to understand the snapshot views of convection as obtained from polar-orbiting satellites (CloudSat being just one example), it is important to place them in a proper dynamic context because different snapshots capture convection at different life stages. Geostationary satellites provide the capability of observing the full life cycle of the convective clouds, which CloudSat only sees with one passing glimpse at a certain life stage. Therefore, we analyze CloudSat depiction of tropical ODC properties and behaviors with convective evolution in mind, adding the otherwise missing time dimension to the CloudSat observations from using ISCCP-CT data.

[5] This paper is organized as follows. Data and methodology are described in section 2. Analysis results and interpretations are presented in section 3. Emphasis is placed on CloudSat depiction of the internal vertical structure of tropical ODC and life cycle view of the tropical ODC based on joint analysis of CloudSat and ISCCP-CT data. Section 4 summarizes the study.

2. Data and Methodology

[6] About 2 years (September 2006 to June 2008) of CloudSat data (2B-GEOPROF and European Centre for Medium-Range Weather Forecasts (ECMWF)-AUX products), together with the International Satellite Cloud Climatology Project (ISCCP) Convection Tracking (CT) database, are used to characterize tropical overshooting deep convection and the cloud systems in which they are embedded. Although CloudSat data extend beyond June 2008, ISCCP-CT data have not yet been updated. September 2006 to June 2008 is the overlapping period. During this period, about 680,000 tropical ODC profiles from CloudSat radar reflectivities are observed (see section 2.2 for selection of ODC). When ISCCP-CT is extended beyond June 2008, we plan to update the analysis.

2.1. Satellite Observations

[7] CloudSat is a member of the A-Train constellation, which consists of a suite of polar-orbiting satellites with an equator crossing time ~1:30 A.M./P.M. [*L'Ecuyer and Jiang*, 2010]. The CloudSat carries a 94 GHz cloud-profiling radar (CPR), which is sensitive to both cloud-size and precipitation-size particles. The footprint of CloudSat is about 1.7 km along track and 1.3 km across track, and the effective vertical resolution is 480 m with oversampling at 240 m resolution. Further details about the CloudSat mission can be found in *Stephens et al*. [2008] or the CloudSat Data Processing Center webpage at http://cloudsat.cira.colostate.edu. Here we mainly use 2B-GEOPROF and ECMWF-AUX data products to characterize tropical ODC. The 2B-GEOPROF product offers cloud mask and radar reflectivity, and ECMWF-AUX product provides temperature and moisture profiles from the European Centre for Medium-Range Weather Forecasts (ECMWF) operational analysis interpolated in time and space to the CloudSat track.

[8] The ISCCP-CT database is derived from geostationary satellite data. Based on the ISCCP pixel-level data (DX), spatially sampled at 30 km intervals, a convective system database has been constructed by clustering all adjacent cold IR pixels with

Table 2. Median Values of LNB, CTH, OSD, and CTETD of ODC for Tropical Ocean and Land and for Five Different Regions (See Figure 4 for the Definition of the Regions)[a]

Median (STD)	LNB	CTH	OSD	CTETD 0 dB*Z*	CTETD 10 dB*Z*
Ocean	13,085 (1,386)	14,591 (1,280)	1,199 (788)	2,398 (1,653)	4,797 (2,354)
Land	12,495 (1,446)	14,516 (1,299)	1,679 (1,073)	2,158 (1,545)	4,317 (2,243)
Africa	12,349 (1,481)	14,514 (1,310)	1,918 (1,127)	2,159 (1,502)	4,317 (2,126)
Amazon	12,723 (1,368)	14,580 (1,211)	1,439 (1,003)	2,158 (1,534)	4,556 (2,250)
TWP	13,657 (1,256)	15,169 (1,039)	1,200 (858)	2,638 (1,761)	5,276 (2,420)
EP ITCZ	12,747 (1,136)	14,235 (992)	1,439 (759)	2,398 (1,516)	4,557 (2,213)
Atlantic ITCZ	12,647 (1,021)	14,078 (943)	1,199 (689)	2,158 (1,471)	4,317 (2,162)

[a]Numbers in the parentheses are the standard deviations (unit: m).

brightness temperature (TB_{IR}) < 245 K [*Machado and Rossow*, 1993]. Such clusters are referred to as Convective Systems (CSs), whether or not they actually contain convective clouds. A further test identifies Convective Clusters as adjacent cloud pixels with TB_{IR} < 220 K. CSs are usually irregular in shape, so to make the results tractable, *Machado et al*. [1998] modeled each CS as an ellipse with the same area and recorded the structural and radiative properties. Once CSs are identified, *Machado et al*. [1998] developed a procedure to track the evolution of each individual CS based on areal overlap between CS in consecutive images. This makes the Convective Tracking (CT) data set that includes the whole CS family. Due to sampling interval of the ISCCP-DX data, the minimum radius size of the CSs that can be tracked is about 90 km. The ISCCP-CT product currently covers the period from July 1983 to June 2008. The data and the document describing the data set are available at http://isccp.giss.nasa.gov/cgi-bin/CT.pl.

2.2. Selection of Overshooting Deep Convection

[9] ODC can be identified from satellite observations using a number of methods. The most commonly used method draws upon IR measurements because overshoots appear as cold pixels in the IR imageries [e.g., *Gettelman et al*., 2002; *Rossow and Pearl*, 2007; *Bedka et al*., 2010, 2012]. Passive microwave measurements can also be used to identify ODC [*Hong et al*., 2005]. Active sensing systems provide the profiling capability, and in the past, TRMM PR observations have been utilized to study the penetrative deep convection [e.g., *Alcala and Dessler*, 2002; *Liu and Zipser*, 2005]. But since TRMM PR is only sensitive to large precipitating particles (sensitivity at ~18 dB*Z*), it generally underestimates the heights of the overshoots. In this study, we use measurements from the CloudSat CPR.

[10] By definition, ODC refers to deep convective plumes that overshoot the level of neutral buoyancy (LNB). So the first step is to find a proper way to define the LNB. The classic definition of LNB is derived from the parcel theory by lifting a near-surface air parcel adiabatically without any dilution to the upper troposphere where it starts to lose buoyancy (called LNB_sounding). LNB can also be determined observationally by observing the actual outflow of deep convection (called LNB_observation). *Takahashi and Luo* [2012] compared the two versions of LNB using sounding (ECMWF analysis) and observations (CloudSat); it was found that LNB_sounding is a reasonable upper bound for LNB_observation, with the former being ~ 800 m higher than the latter because entrainment of environmental air dilutes the convective ascent thus lowering the height of convective outflow. Considering that using LNB_observation severely limits the sample size (only 4800 cases are found from 2.5 years of CloudSat data, mainly from the west pacific) for global survey of ODC, in this study we calculate LNB from the ECMWF-AUX data (i.e., LNB_sounding) and use it as the reference level for selecting ODC: Any convective tower observed by CloudSat that extends above the corresponding LNB by some threshold is defined as ODC. For the tropics (30°S–30°N), LNB for the selected ODC ranges from 12.3 to 13.7 km, depending on locations (Table 2).

[11] The exact procedure for selecting ODC goes as follows: First, deep convection is identified from CloudSat 2B-GEOPROF data in a way similar to *Takahashi and Luo* [2012]. The requirements are (1) cloud top height (CTH) ≥ 10,000 m, (2) cloud-based height (CBH) ≤ 2000 m, (3) continuity in radar echo from CBH to CTH to exclude nonconvective, layered clouds. CPR Cloud Mask ≥ 20 (20 or higher indicates high confidence in cloud detection; note that cloud mask value is not to be confused with radar reflectivity) is required, as in *Riley and Mapes* [2009] and *Bacmeister and Stephens* [2011]. Second, the corresponding LNB is calculated from the collocated ECMWF-AUX data assuming pseudoadiabatic ascent from the planetary boundary layer. Finally, ODC is defined as any convective profile from CloudSat CPR with CTH > LNB + δ, where δ = 500 m. Choice of 500 m for δ is meant to match previous studies such as *Bedka et al*. [2010] so that meaningful comparison can be made. We have experimented δ from 0 to 1300 m. The final choice of δ = 500 m provides ODC statistics that agree broadly with previous studies. Figure 1 gives an example of how ODC is selected. Figure 1 (top) shows the IR brightness temperature (a proxy for cloud top temperature) from Moderate Resolution Imaging Spectroradiometer (MODIS). The dotted line indicates the CloudSat footprint. Figure 1 (bottom) shows the vertical distribution of radar reflectivity from CloudSat. The black line is the height of LNB, and the arrows point to the locations of the selected overshooting features.

2.3. Proxies of Convective Strength

[12] CloudSat CPR offers some unique views of ODC. Its high sensitivity to both cloud and precipitating particles and profiling capability give a glimpse into the internal vertical structure of ODC and also allows for the identification of convective strength. Here we define three proxies for convective strength. The first proxy is radar echo top height (ETH) of large echoes, following *Luo et al*. [2008]. ETH of 0 dB*Z* (10 dB*Z*) is the highest altitude that 0 dB*Z* (10 dB*Z*) radar echo reaches. Strong updraft tends to produce high ETH, i.e., large particles being lofted to greater altitude. It should be pointed out that attenuation of radar reflectivity is negligible when

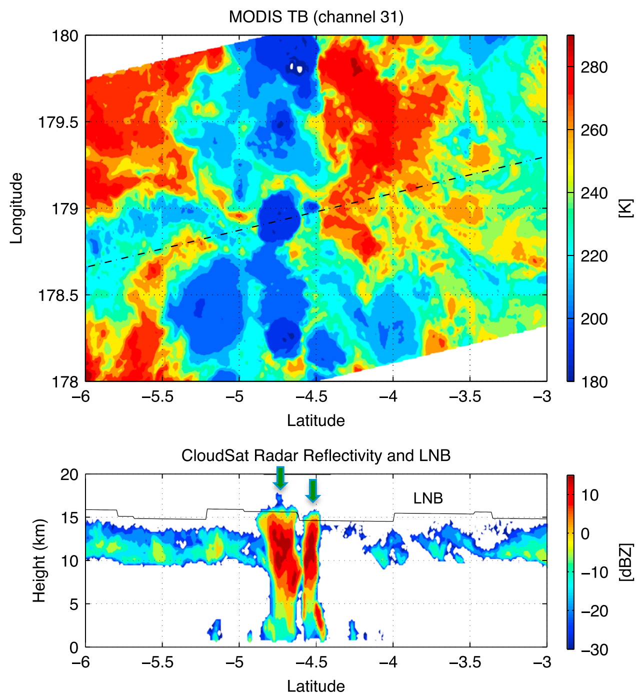

Figure 1. Example of overshooting features from different satellite view. (top) MODIS provides the plan view of the brightness temperature (a proxy of cloud top temperature), while (bottom) CloudSat provides vertical distribution of radar refractivity and cloud properties. The dotted line (Figure 1, top) indicates that CloudSat footprint. The black line (Figure 1, bottom) is the height of LNB, and the arrows point to the locations of the selected ODC.

one searches the highest level of 10 dB*Z* and 0 dB*Z* from cloud top downward; for deep convective clouds, these high ETHs are usually found near cloud top well above the melting levels. The second proxy is called overshooting distance (OSD), defined as the difference between CTH (which roughly corresponds to the ETH of about –30 dBZ) and LNB. OSD describes the extra distance by which a deep convective plume overshoots the corresponding LNB. Intuitively, it is indicative of the convective strength or intensity since stronger convective plumes overshoot higher. Extremely strong deep convection can penetrate directly into the stratosphere, much higher than the LNB [e.g., *Luo et al.*, 2008]. The third proxy is called cloud top-echo top distance (CTETD), which is defined as the distance between CTH and ETH of 0 dB*Z* and 10 dB*Z*. When convection is strong, both small and large particles are lofted to higher altitude, so CTH and ETH are similar (thus, small CTETD). On the other hand, if convection is weak, large particles fall short of the cloud top resulting in large CTETD. Figure 2 uses schematics to illustrate these different proxies.

2.4. Definition of Convective Life Stage

[13] ISCCP-CT database gives CloudSat snapshots the missing time dimension so that we are able to identify the life stage of CSs in which ODC is embedded. Following *Futyan and Del Genio* [2007], we use two independent variables, coldest IR brightness temperature (TB_{IR}) and radius size (R) of the CS, to determine the life stages of the convective system. We define it as the "developing stage" if the system has not reached the minimum TB_{IR} (i.e., highest CTH) of its lifetime and as the "dissipating stage" if the system has already passed its maximum size. The life stage between the developing stage and the dissipating stage is defined as the "mature stage." The rationale for the life stage classification is that CSs are expected to develop vertically first and then expand horizontally. To smooth out abrupt changes in TB_{IR} and R, we apply a polynomial curve fitting and use F test to determine the best order fit. Due to the temporal and spatial resolutions of the ISCCP-CT data (3 h and 30 km, respectively), only CSs whose lifetimes are longer than 6 h (i.e., a minimum of three geostationary images) and whose radiuses are larger than 90 km have been used (section 3.3). Three-hourly CT data are interpolated when there is only one missing image between the consecutive images and then further interpolated to hourly intervals. But it should be noted that the deep convective clouds analyzed in sections 3.1 and 3.2 are not constrained by the large system condition; they include all CloudSat observations.

[14] Depending on the time at which CloudSat-observed ODC intercepts the ISCCP-CT data, it is assigned a given life

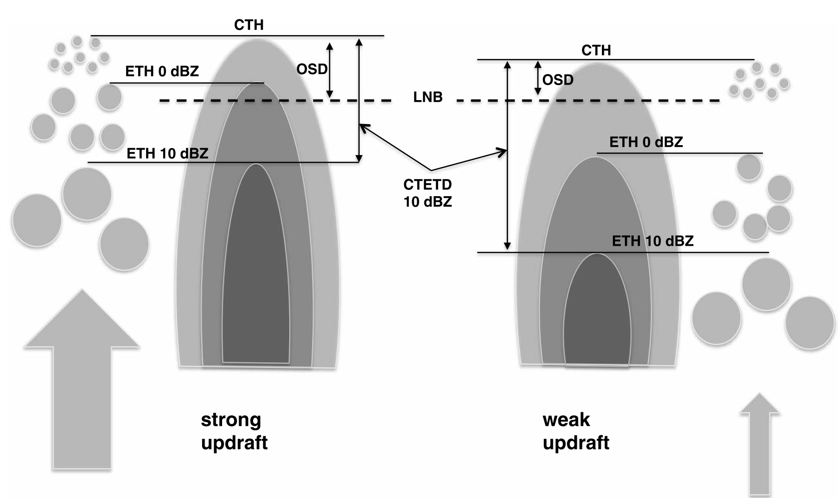

Figure 2. Schematics showing the three proxies of convective strength (ETH, OSD, and CTETD) for strong and weak updrafts.

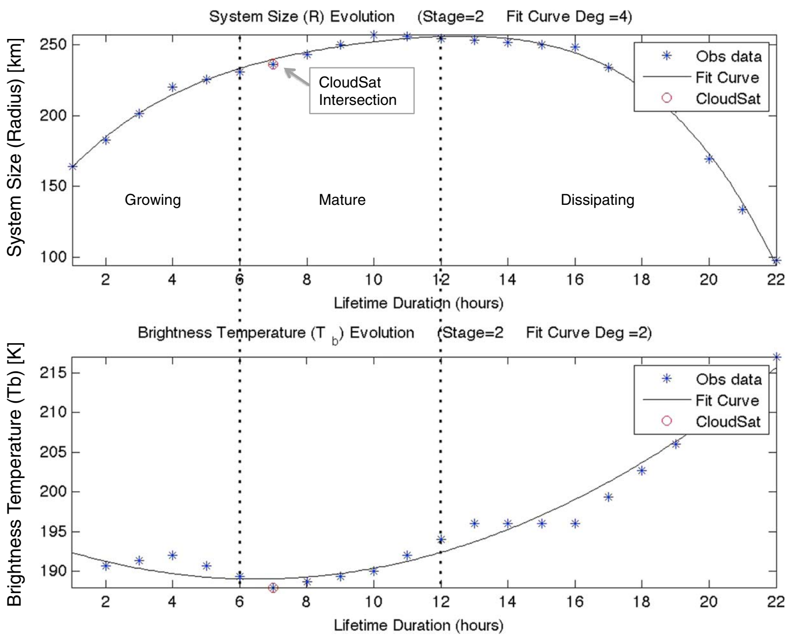

Figure 3. An example of the "growing stage," "mature stage," and "dissipating stage" classified by system radius and minimum brightness temperature. The curve shows the best fitting based on an *F* test.

stage—developing, mature, or dissipating. Figure 3 illustrates the overall methodology using an example of ODC embedded in the mature stage of the CS.

3. Results

3.1. Tropical ODC Climatology and Regional Variations: A CloudSat Perspective

[15] In this section, we present a CloudSat depiction of tropical ODC climatology and regional variations, since this has not been done before. CloudSat CPR provides a new perspective of these clouds that complements previous observations using IR, passive microwave, and precipitation radar, although the fixed sampling time (around 1:30 A.M./P.M. local time) introduces certain biases.

[16] We first examine deep convection (DC) in general (i.e., convective clouds with CTH > 10 km; see section 2 for definition): the occurrence frequency of DC by CloudSat is about 2.2% over whole tropics (30°S to 30°N) (Occurrence frequency of DC is defined as the number of DC profiles divided by the total number of CloudSat profiles, including clear scenes. Other occurrence frequencies are defined in a similar fashion.). It becomes ~3.1% if we only count 15°S to 15°N. This number is slightly lower than the statistics given by *Luo et al.* [2008], which is 3.9% based on CloudSat 2B-CLDCLASS data due to slightly different definition of DC. Note that the CloudSat-based definition of DC only counts those clouds that are rooted in the planetary boundary layer (PBL) and does not include the attached anvils because active sensors can effectively separate convective plumes from the anvils based on radar profiles. This is different from most IR-based definition of DC in which it is difficult to differentiate thick anvils from active convection because they may both show similar cold temperatures. Caution should thus be taken when comparing these different climatologies.

[17] ODC is a small subset of DC. Statistics of ODC depends on the choice of the reference level (i.e., LNB) and the overshooting distance (δ). Figure 4 (first panel) shows the climatology of LNB based on collocated ECMWF analyses. Figure 4 also shows the occurrence frequency of ODC with different δ values: The occurrence frequency of ODC varies from 0.24% to 0.65% over 30°S–30°N and 0.36% to 0.97% over 15°S–15°N when δ varies from 0 m to 1300 m (bottom four panels). Larger δ leads to fewer ODC. In this study, we use $\delta = 500$ m, following the reasoning described in section 2.2. Under this definition, the occurrence frequency of ODC is 0.46% over 30°S–30°N and 0.69% for 15°S and 15°N. So considering that the DC occurrence frequency is 2.2% (30°S–30°N), our result shows that approximately 21% of tropical DC has overshooting tops, which is comparable to the statistic given by *Hong et al.* [2005] who found that 26% of tropical DC has overshooting tops. Again, we emphasize that DC here refers to those active convective plumes rooted in the PBL, not including the attached anvils.

[18] Of particular interest are the ODC events that have the potential to directly penetrate into the lower stratosphere, which we call penetrative deep convection. *Luo et al.* [2008] studied the convective life cycle and internal vertical structures of such penetrative deep convection. Our result here shows that only ~1% of tropical DC (i.e., ~0.0002 of the tropical region) has overshooting tops higher than 16.5 km, which is about the mean height of the cold point tropopause defined by *Gettelman and de F. Forster* [2002]. This result is similar to the statistics as given by *Luo et al.* [2008] and broadly agrees with *Rossow and Pearl* [2007]. The exact role played by these penetrative deep convective events in terms of their impacts on the lower stratospheric heat budget and constituents is not clearly understood [*Fueglistaler et al.*, 2009]. Although the occurrence frequency of 0.0002 is a very small number, the associated contribution to mass and heat fluxes may not be negligible. Moreover, such penetrative transports

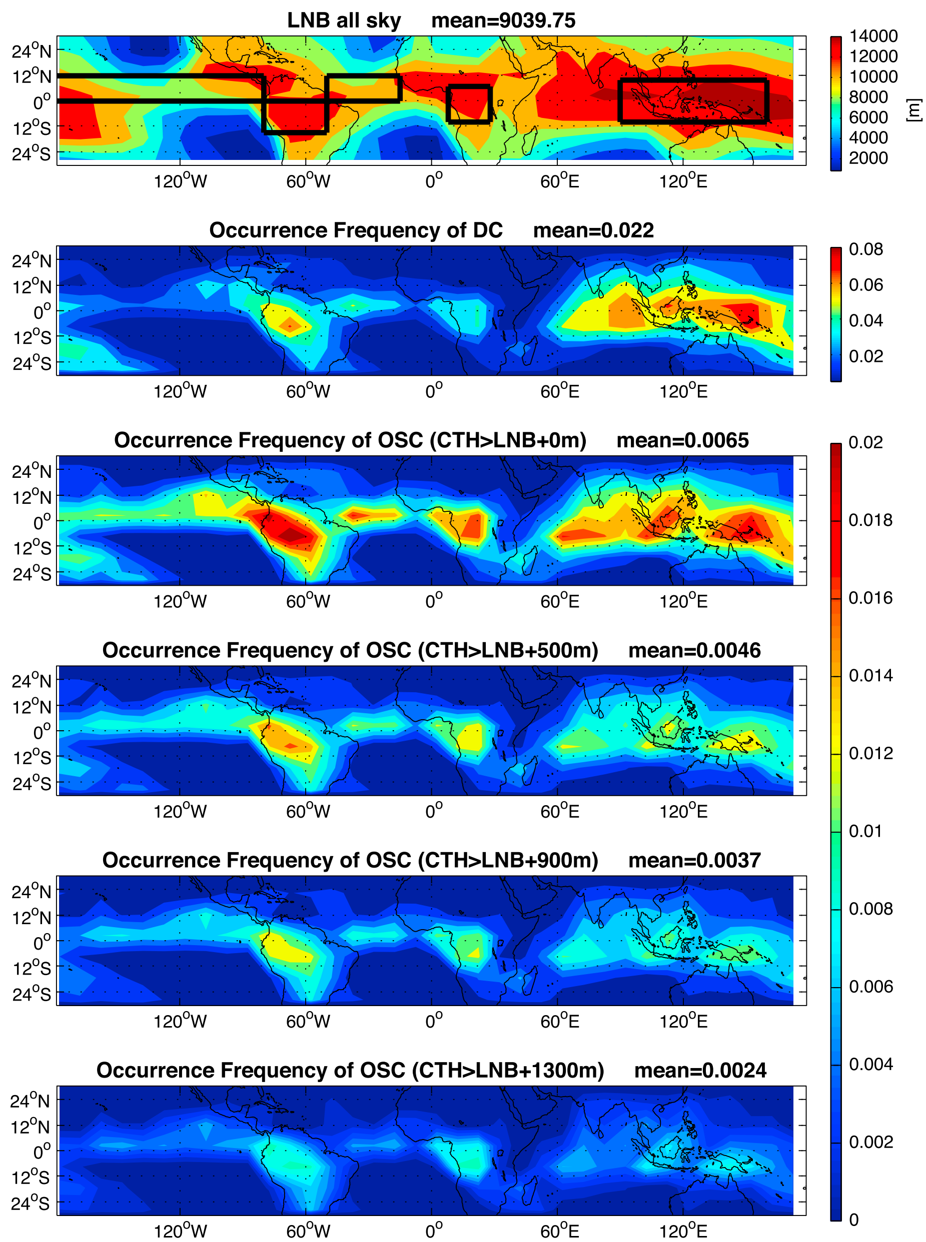

Figure 4. (top to bottom) LNB (unit: m), occurrence frequency of DC, and occurrence frequencies of ODC with different δ values (from 0 to 1300 m). Values are the means within each $10° \times 10°$ grid box. Black solid boxes in the first panel are the five selected regions discussed in the text: tropical Africa, Amazon, tropical warm pool (TWP), eastern Pacific Intertropical Convergence Zone (EP ITCZ), and Atlantic ITCZ.

communicate the PBL with the lower stratosphere in a very short time scale on the order of only 10 min. This is a very different scenario from gentle ascent in the TTL, at least for the chemically active species.

[19] Land-ocean contrasts are also investigated. For our definition of ODC, the occurrence frequencies are similar between land: The ratio of occurrence frequency over land to ocean is 1.01. Taken at face value, this seems to be somewhat at odds with previous work using TRMM PR, which found noticeably more ODC over tropical land than over ocean [e.g., *Liu and Zipser*, 2005]. However, it should be emphasized that CloudSat PR with the sensitivity at ~ -30 dBZ sees small ice crystals at the top of ODC, whereas TRMM PR with sensitivity at ~ 18 dBZ only detects precipitation-size particles. *Liu et al.* [2007] reconciled different views of ODC from TRMM PR and IR measurements, showing that IR measurements have less land-ocean differences. In this regard, CloudSat-detected cloud tops are more similar to those by IR (i.e., high sensitivity to small cloud particles), so its depiction of land-ocean contrast in ODC is comparable to those by IR as in *Gettelman et al.* [2002] and *Rossow and Pearl* [2007].

[20] It is interesting to note that if we choose $\delta = 900$ m, that is, stricter criterion which selects more intense ODC, then land-ocean contrast in ODC occurrence frequencies starts to favor land (the ratio of occurrence frequency over

Table 3. Correlation Coefficiencies Between Different Cloud and Convective Properties

	Whole Tropics	Land	Ocean
CTH versus LNB	0.78	0.70	0.83
CTH versus ETH 0 dB*Z*	0.66	0.73	0.63
CTH versus ETH 10 dB*Z*	0.47	0.56	0.43
LNB versus ETH 0 dB*Z*	0.52	0.53	0.53
LNB versus ETH 10 dB*Z*	0.35	0.40	0.35
OSD versus ETH 0 dB*Z*	0.12	0.16	0.08
OSD versus ETH 10 dB*Z*	0.11	0.12	0.08

land to ocean is 1.25). Pushing δ to the extreme (1300 m), land ODC becomes more dominant over the ocean counterpart (the ratio of occurrence frequency over land to ocean becomes 1.65), suggesting that intense ODC is more prevalent over land, consistent with the finding from TRMM [*Liu and Zipser*, 2005] and passive microwave [*Hong et al.*, 2005], which are known to be more sensitive to large ice particles that are indicative of strong convective updrafts.

[21] Another important factor to consider when comparing our results to those by TRMM and IR is the diurnal cycle. CloudSat makes measurements at around 1:30 A.M./P.M. local time. Tropical deep convection over land has a strong diurnal cycle, and the peak is usually in the late afternoon [*Liu and Zipser*, 2008]. Therefore, CloudSat probably underestimates the occurrence frequency of ODC over land. Deep convection over the ocean, in contrast, has a much smaller diurnal cycle [*Liu and Zipser*, 2008] so less underestimation is expected over the ocean. We will return to the issue concerning the diurnal cycle in section 3.3 when ISCCP-CT data are analyzed in conjunction with CloudSat. ISCCP-CT data provide a full coverage of the diurnal cycle because they are based on geostationary satellite data.

[22] Some regional differences in DC and ODC are worth discussing. Figure 4 shows that DC and ODC are most prevalent over the following five regions: tropical Africa, Amazon, tropical warm pool (TWP), eastern Pacific (EP) Intertropical Convergence Zone (ITCZ), and Atlantic ITCZ (black boxes in Figure 4 define these regions). The occurrence frequencies of DC (ODC) over central Africa, Amazon, TWP, EP ITCZ, and Atlantic ITCZ are, respectively, 3.14% (1.08%), 5.72% (1.52%), 5.39% (0.84%), 2.77% (0.91%), and 3.54% (0.88%). While the overall statistics shows little difference in ODC over land versus over ocean as discussed above, the two land centers of action (tropical Africa and Amazon) have significantly larger occurrence frequencies of ODC than the three oceanic counterparts, even if the continental deep convection has a potential to be underestimated due to the inability to catch the full diurnal cycle.

[23] The regional difference in ODC can be examined in another way, that is, the percentage of DC that overshoots or the ratio of ODC occurrence frequency to that of DC. These percentages or ratios are, respectively, 34.5%, 26.5%, 15.6%, 32.9%, and 25.0% over the five regions (tropical Africa, Amazon, TWP, EP ITCZ, and Atlantic ITCZ). This shows that tropical Africa has the highest ratio and TWP has the lowest. Figure 4 also shows that the western part of tropical Africa has a particularly high concentration of ODC. This is consistent with previous findings that show this region contains the most intense thunderstorms and the highest frequency of lightning flashes [*Zipser et al.*, 2006; *Toracinta and Zipser*, 2001; *Petersen and Rutledge*, 2001]. Those are partly due to the interaction between topographic effects and regional circulation and partly due to the African easterly jet of the Southern Hemisphere [*Jackson et al.*, 2009].

3.2. Convective Cloud Properties Associated With ODC

[24] CloudSat CPR offers a unique view of the internal vertical structures of the ODC, which have not been systematically analyzed before. Here we examine various parameters that are used to characterize cloud structure (e.g., CTH), convective intensity (the three proxies defined in section 2.3 and schematically shown in Figure 2: ETH, OSD, and CTETD), and convective environment (e.g., LNB), as well as the relationship among them.

[25] Table 2 summarizes some of these parameters associated with ODC for tropical land and ocean, and the five regions as defined in Figure 4. In general, LNB is higher over ocean than land (13,085 m versus 12,495 m). CTHs of the ODC are similar over land and ocean (14,516 m versus 14,591 m). Convective intensity is consistently stronger over land than over ocean as indicated by OSD, CTETD for 0 dB*Z* and CTETD for 10 dB*Z*, even though CloudSat overpass time (~1:30 A.M./P.M. local time) does not fully capture the afternoon peak of the continental deep convection.

[26] Among all five regions, tropical Africa shows the strongest convective intensity with the largest OSD and the smallest CTETD. ODC over the TWP has the weakest intensity based on these measures. The contrast in convective intensity between tropical Africa and TWP has also been studied by *Liu and Zipser* [2005] using TRMM PR; their conclusion is similar to ours using CloudSat CPR. This suggests that large echoes from CloudSat CPR (0 dB*Z* and 10 dB*Z*) are capable of identifying convective strength, in a way similar to TRMM PR. However, it should be pointed out that since CPR has sensitivity all the way down to -30 dB*Z*, it is also capable of observing small cloud droplets and ice crystals and thus gives a more complete depiction of the whole vertical structure of the convective system. For example, Table 2 shows that smaller cloud particles as represented by CPR CTH (i.e., -30 dB*Z* ETH) reach a higher altitude over TWP (15,169 m) than tropical Africa (14,514 m), despite the fact that large rain-size particles as represented by ETH of 10 dB*Z* show the opposite contrast. In other words, the highest altitudes reached by cloud-size particles and rain-size particles show different regional contrast.

[27] *Lucas et al.* [1994] discussed possible reasons for stronger land convection: Although the absolute values of CAPE (convective available potential energy) do not differ much between land and ocean, their shapes are quite different: oceanic convection has “skinny” CAPE (i.e., the associated positive area of CAPE is narrow but deep), whereas continental convection tends to have “fat” CAPE (i.e., the associated positive area of CAPE is wide but less deep). The latter shape can more effectively accelerate ascending air parcels to higher vertical velocity. *Zipser* [2003] offered another possible explanation: Glaciation of water droplets when they are transported to the upper troposphere adds additional latent heat to the air parcels, reinvigorating the convection. Land convection with higher aerosol concentration tends to delay warm rain and transports more water droplets to the higher levels where they glaciate.

Table 4. Normalized Occurrence Frequencies of ODC for the Three Stages

		Ocean		Land	
Stages	All Cases	Noon (13:30)	Midnight (1:30)	Noon (13:30)	Midnight (1:30)
Growing	66.2%	74.1%	74.7%	66.0%	72.7%
Mature	33.4%	25.8%	24.9%	33.5%	26.6%
Dissipating	0.4%	0.1%	0.4%	0.4%	0.7%

[28] Correlations between various parameters used to characterize convective properties are summarized in Table 3. A few results deserve discussion.

[29] 1. Relatively high correlation (0.78) is seen between CTH and LNB, suggesting that the vertical development of ODC tends to follow LNB. Correlation coefficient is higher over ocean (0.83) than over land (0.70).

[30] 2. CTH and ETH (both 0 dB*Z* and 10 dB*Z*) are also positively correlated, although the correlation coefficients are smaller than that between CTH and LNB. This suggests that convective strength (as indicated by ETH) and cloud depth (CTH) are closely related. Unlike the relationship between CTH and LNB, larger correlations between CTH and ETH are found over land than over ocean. These differences may reflect different dynamical and microphysical processes controlling cloud-size particles (represented by CTH) and precipitation-size particles (represented by ETH).

[31] 3. LNB and ETH are also positively correlated, but the correlation coefficients are generally lower than those for LNB and CTH and for CTH and ETH. Recall that LNB can be thought of as reflecting the environmental condition that caps the deep convective development [*Takahashi and Luo*, 2012]. Our results suggest that this "capping" effect is stronger for CTH (i.e., cloud-size particles) than for ETH (i.e., precipitation-size particles).

[32] 4. Another parameter pertaining to ODC is the OSD, which also measures convective intensity but from a different perspective than ETH. Table 3 shows that the correlation between OSD and ETH are relatively small. One possible reason may have to do with vertical wind shear: Since ETH and OSD are recorded profile by profile (1.7 km along track and 1.3 km across track), vertical wind shear may displace the overshooting top horizontally from the precipitation ETH, affecting the one-to-one correlation between OSD and ETH. However, when averaged over a large region for many ODC events, OSD and ETH tend to give a consistent depiction of the convective intensity.

3.3. Life Stages of ODC

[33] A unique aspect of this ODC study is the combination of CloudSat with geostationary satellite data. That is, each snapshot of ODC by CloudSat is cast in the context of the whole life cycle of the convective system (CS) in which it is embedded. Using size (*R*) and the minimum TB_{IR} of the CS from the ISCCP-CT database, we define three convective life stages: growing, mature, and dissipating as described in section 2.4 (see also Figure 3).

[34] We first investigate the question at which life stage(s) of the systems are the ODC events most preferably observed. We find that 81% of the matched ODC cases are embedded at the growing stage of the CSs, 18% of the cases at the mature stages, and only 1% of the cases at the dissipating stages. However, the lifetime duration of each stage is different: If the entire lifetime is normalized to 1, the average lifetime durations at growing, mature, and dissipating stages are 0.35, 0.16, and 0.49, respectively. To avoid sampling bias among each stage, we normalize the results by dividing the total number of ODC events embedded in each life stage by the lifetime duration of that stage. After this adjustment, our result shows that ODC occurs predominately during the growing stage of the CSs (~66.2% of all matched ODC cases), the mature stage comes second (~33.4%), and only very few ODC cases (~0.4%) are found during the dissipating stage (Table 4). It is interesting to see that about one third of ODC is found at the mature stage of the CSs. This suggests that although the convective systems start to detrain and develop anvils, many of them still experience strong updrafts that overshoot. The dissipating stage is the period of decaying during which cloud tops get warmer (CTH starts decreasing) with time and size becomes smaller. Hence, ODC can hardly occur at this stage.

[35] We break down the statistics by land and ocean and by daytime (~13:30 local time) and nighttime (~1:30 local time) overpasses (Table 4). Partitions of ODC events for each life stage over ocean appear to show little variation between daytime and nighttime. In other words, little diurnal variation is observed over ocean. Over land, ODC is less concentrated at the growing stage during the daytime than the nighttime, that is, the mature stage has more share of ODC events during the day than during the night. This can be interpreted as related to the diurnal cycle of convective intensity: Stronger land convection in the afternoon time may sustain ODC plumes well

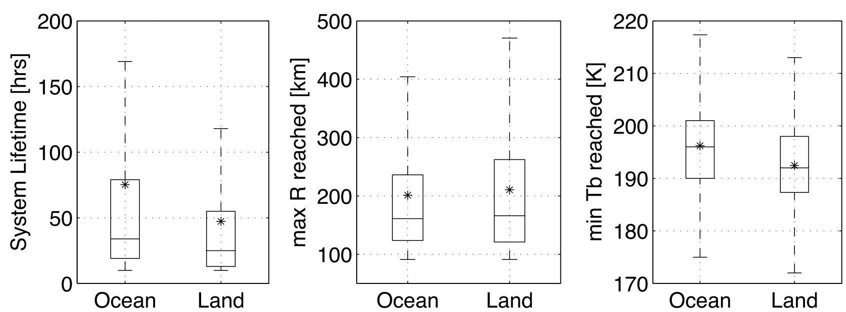

Figure 5. (left) Box diagram for the system lifetime, (middle) peak system sizes reached, and (right) the minimum brightness temperature reached. The bottom and top of the boxes show, respectively, the 25% and 75% percentile. The central lines show the median, and stars inside the box show the mean. The ends of dashed lines are the minimum and maximum.

Table 5. Median Values of ETH, OSD, and CTETD for the ODC Events Embedded in the Growing and Mature Stages of the CSs[a]

Median (STD)	Ocean/Land	ETH 0 dB*Z*	ETH 10 dB*Z*	OSD	CTETD 0 dB*Z*	CTETD 10 dB*Z*
Growing	Ocean	12,075 (1,987)	9,448 (2,296)	1,114 (523)	2,533 (1,471)	5,036 (1,983)
	Land	12,143 (2,051)	9,747 (2,219)	1,558 (919)	2,222 (1,285)	4,653 (1,880)
Mature	Ocean	11,200 (2,044)	8,903 (2,465)	1,106 (585)	2,744 (1,512)	5,120 (2,103)
	Land	11,602 (2,210)	9,470 (2,415)	1,559 (832)	2,278 (1,473)	4,588 (1,842)

[a]Numbers in the parentheses are the standard deviations (unit: m).

into the mature stage of the convective system [e.g., *Chung et al*., 2007].

[36] It is also of interest to examine the character of the convective systems in which ODC events are embedded. Figure 5 shows the statistics of the system lifetime, max *R*, and the min TB_{IR} (max *R* and min TB_{IR} are used to define life stages; see Figure 3). Max *R* is slightly larger over land than over ocean (but statistically insignificant at 95% confidence level). There are some larger differences in the distribution of lifetime and min TB_{IR} between oceanic and continental convection (both statistically significant at 95% confidence level). Oceanic convection has longer lifetimes than continental convection: The mean and median for the ocean cases are, respectively, 75.3 h and 34 h, while the values for land cases are, respectively, 47.2 h and 25 h. Continental convection tends to have colder min TB_{IR} (mean and median are both at 192 K) than oceanic convection (mean and median are both at 196 K).

[37] Finally, we analyze convective strengths of the ODC embedded in different life stages of the convective systems (Table 5). Since ODC is rarely found in the dissipating stage (only 0.4% of all cases) and as such no enough statistics can be compiled, we only compare the growing stage and the mature stage. Almost all proxies in Table 5 point to stronger convective intensity for ODC during the growing stage, that is, larger ETH (both 0 dB*Z* and 10 dB*Z*), larger OSD, and smaller CTETD. This suggests that the "vigor" of the embedded overshooting convective cell and the life stage of the whole convective systems are well correlated.

[38] Note that this section only discusses the character of the convective systems that contain ODC, which is the focus of the current study. Early publication by *Machado et al.* [1998] described the life cycle characteristics of deep convective systems in general (i.e., with or without overshooting turrets) over the Americas using GOES-7 satellite data. Our ongoing research seeks to expand the survey to the whole globe, given that ISCCP-CT data are now global.

4. Summary and Discussions

[39] Tropical overshooting deep convection (ODC) plays a critical role in affecting the heat and moisture budgets of the upper troposphere and lower stratosphere. Understanding these important influences requires, in part, ways of observing the tropics-wide distribution of ODC as well as their properties and behaviors. A number of satellite-based studies have been conducted in the past using, for example, IR, passive microwave, and precipitation radar measurements. This current study approaches the subject from a few different angles, emphasizing (1) the new and unique observations from the CloudSat cloud-profiling radar (CPR) and (2) the synergy between CloudSat snapshots and the whole convective life cycle as provided by geostationary satellite observations. The latter information is provided by the ISCCP Convection tracking (CT) database based on three-hourly pixel-level geostationary data that give the life stage information of the convective system in which ODC events are embedded. The principal findings are briefly summarized as follows.

[40] (1) The occurrence frequency of ODC based on CloudSat observations is approximately 0.46% between 30°S and 30°N and 0.69% between 15°S and 15°N. There is little overall land-ocean difference, broadly consistent with previous statistics using IR measurements. However, when the criteria for selecting ODC become stricter with requirements of not only cloud top height but also strong convective intensity, the land-ocean partition starts to favor land, consistent with previous studies using TRMM PR and passive microwave measurements.

[41] (2) Regional variations in tropical ODC are investigated. Two contrasting regions are tropical warm pool (TWP) and tropical Africa: While the former has larger occurrence frequency of deep convection (DC) in general, the latter has larger occurrence frequency of ODC. The Amazon region is abundant in both DC and ODC. Caution, however, should be exercised to interpret these results because of the fixed sampling time (~ 1:30 and 13:30 local time). For example, the lower CTH of tropical Africa may be because the diurnal peak is missed.

[42] (3) CloudSat CPR offers a unique view of the internal vertical structure of ODC, which has not been systematically documented before. We analyze various parameters that are used to characterize cloud vertical extent (CTH), convective intensity (ETH, OSD, and CTETD), and convective environment (LNB). Among all the regions, tropical Africa shows the strongest convective intensity. Correlations between these various parameters are also computed, showing generally close relationship among convective environment, cloud vertical development, and convective strength.

[43] (4) ISCCP-CT data are analyzed to identify the life stage of the convective system (CS) in which ODC events are embedded. It was found that ODC occurs predominantly during the growing stage of the CSs (66.2%), the mature stage comes second (33.4%), and only very few ODC cases are found during the dissipating stage (0.4%). There is little variation in the statistics between daytime (13:30) and nighttime (1:30) overpasses for oceanic cases; for land cases, the mature stage has more share of ODC during the day than during the night (see Table 4). Convective intensity is compared between the growing and mature stages: Almost all proxies point to stronger ODC during the growing stage.

[44] This paper builds upon previous works and continues to elucidate the properties and behaviors of tropical ODC. The novel aspect of the study is that the CloudSat depiction of ODC is cast in the dynamic context provided by the geostationary satellite observations. The life stage view of ODC has important implications for mechanistic studies of tropical ODC and its influence on heat and constituent budgets of the

upper troposphere and lower stratosphere. For example, knowing that ODC events are found predominantly in the growing stage of the CSs, future observational (e.g., field campaign) and modeling studies should therefore focus on the early duration of the system. The finding of the land-ocean and day-night differences is also intriguing. Detailed studies should be planned to understand why over land, a larger proportion of the daytime ODC events occurs during the mature stage than at night, but no such contrast is seen for oceanic CSs.

[45] **Acknowledgments.** The study was supported by two NASA grants awarded to CUNY: NNX10AM31G and NNX12AC13G. The ISCCP-CT data were kindly provided by Cindy Pearl. The authors would like to thank William Rossow and Jonathan H. Jiang for insightful comments and discussions. We also want to thank Jeyavinoth Jeyaratnam for computational assistance.

References

Alcala, C. M., and A. E. Dessler (2002), Observations of deep convection in the tropics using the Tropical Rainfall Measuring Mission (TRMM) precipitation radar, *J. Geophys. Res.*, *107*(D24), 4792, doi:10.1029/2002JD002457.

Bacmeister, J. T., and G. L. Stephens (2011), Spatial statistics of likely convective clouds in CloudSat data, *J. Geophys. Res.*, *116*, D04104, doi:10.1029/2010JD014444.

Bedka, K. M., J. Brunner, R. Dworak, W. Feltz, J. Otkin, and T. Greenwald (2010), Objective satellite-based overshooting top detection using infrared window channel brightness temperature gradients, *J. Appl. Meteorol. Climatol.*, *49*, 181–202.

Bedka, K. M., R. Dworak, J. Brunner, and W. Feltz (2012), Validation of satellite-based objective overshooting cloud-top detection methods using CloudSat cloud profiling radar observations, *J. Appl. Meteorol. Climatol.*, *51*, 1811–1822.

Bergman, J., E. Jensen, L. Pfister, and Q. Yang (2012), Seasonal differences of vertical-transport efficiency in the tropical tropopause layer: On the interplay between tropical deep convection, large-scale vertical ascent, and horizontal circulations, *J. Geophys. Res.*, *117*, doi:10.1029/2011JD016992.

Chung, E.-S., B.-J. Sohn, J. Schmetz, and M. Koenig (2007), Diurnal variation of upper tropospheric humidity and its relations to convective activities over tropical Africa, *Atmos. Chem. Phys.*, *7*, 2489–2502.

Chung, E.-S., B.-J. Sohn, and J. Schmetz (2008), CloudSat shedding new light on high reaching tropical deep convection observed with Meteosat, *Geophys. Res. Lett.*, *35*, L02814, doi:10.1029/2007GL032516.

Fueglistaler, S., A. E. Dessler, T. J. Dunkerton, I. Folkins, Q. Fu, and P. W. Mote (2009), Tropical tropopause layer, *Rev. Geophys.*, *47*, RG1004, doi:10.1029/2008RG000267.

Futyan, J. M., and A. D. Del Genio (2007), Deep convective system evolution over Africa and the tropical Atlantic, *J. Clim.*, *20*, 5041–5060.

Gettelman, A., and P. M. de F. Forster (2002), A climatology of the tropical tropopause layer, *J. Meteorol. Soc. Jpn.*, *80*(4B), 911–924.

Gettelman, A., M. L. Salby, and F. Sassi (2002), The distribution and influence of convection in the tropical tropopause region, *J. Geophys. Res.*, *107*(D10), 4080, doi:10.1029/2001JD001048.

Hong, G., G. Heygster, J. Miao, and K. Kunzi (2005), Detection of tropical deep convective clouds from AMSU-B water vapor channels measurements. *J. Geophys. Res.*, *110*, D05205, doi:10.1029/2004JD004949.

Iwasaki, S., T. Shibata, J. Nakamoto, H. Okamoto, H. Ishimoto, and H. Kubota (2010), Characteristics of deep convection measured by using the A-Train constellation, *J. Geophys. Res.*, *115*, D06207, doi:10.1029/2009JD013000.

Iwasaki, S., T. Shibata, H. Okamoto, H. Ishimoto, and H. Kubota (2012), Mixtures of stratospheric and overshooting air measured using A-Train sensors, *J. Geophys. Res.*, *117*, D12207, doi:10.1029/2011JD017402.

Jackson, B., S. E. Nicholson, and D. Klotter (2009), Mesoscale convective systems over western equatorial Africa and their relationship to large-scale circulation, *Mon. Weather Rev.*, *137*, 1272–1294.

Jiang, J. H., B. Wang, K. Goya, K. Hocke, S. D. Eckermann, J. Ma, D. L. Wu, and W. G. Read (2004), Geographical distribution and interseasonal variability of tropical deep convection: UARS MLS observations and analyses, *J. Geophys. Res. 109*, D03111, doi:10.1029/2003JD003756.

Jiang, J. H., N. J. Livesey, H. Su, L. Neary, J. C. McConnell, and N. A. Richards (2007), Connecting surface emissions, convective uplifting, and long-range transport of carbon monoxide in the upper troposphere: New observations from the Aura Microwave Limb Sounder, *Geophys. Res. Lett.*, *34*, L18812, doi:10.1029/2007GL030638

Kuang, Z. M., and C. S. Bretherton (2004), Convective influence on the heat balance of the tropical tropopause layer: A cloud-resolving model study, *J. Atmos. Sci.*, *61*(23), 2919–2927.

Küpper, C., J. Thuburn, G. C. Craig, and T. Birner (2004), Mass and water transport into the tropical stratosphere: A cloud-resolving simulation, *J. Geophys. Res.*, *109*, D10111, doi:10.1029/2004JD004541.

L'Ecuyer, T., and J. H. Jiang (2010), Touring the atmosphere aboard the A-Train, *Phys. Today*, *63*(7), 36–41.

Liu, C., and E. J. Zipser (2005), Global distribution of convection penetrating the tropical tropopause, *J. Geophys. Res.*, *110*, D23104, doi:10.1029/2005JD006063.

Liu, C., and E. J. Zipser (2008), Diurnal cycles of precipitation, clouds, and lightning in the tropics from 9 years of TRMM observations, *Geophys. Res. Lett.*, *35*, L04819, doi:10.1029/2007GL032437.

Liu, C., E. J. Zipser, and S. W. Nesbitt (2007), Global distribution of tropical deep convection: Different perspectives from TRMM infrared and radar data, *J. Clim.*, *20*, 489–503.

Lucas, C., E. Zipser, and M. A. LeMone (1994), Vertical velocity in oceanic convection off tropical Australia, *J. Atmos. Sci.*, *51*, 3183–3193.

Luo, Z., G. Y. Liu, and G. L. Stephens (2008), CloudSat adding new insight into tropical penetrating convection, *Geophys. Res. Lett.*, *35*, L19819, doi:10.1029/2008GL035330.

Luo, Z., G. Y. Liu, G. L. Stephens, and R. H. Johnson (2009), Terminal versus transient cumulus congestus: A CloudSat perspective, *Geophys. Res. Lett.*, *36*, L05808, doi:10.1029/2008GL036927.

Luo, Z. J., G. Y. Liu, and G. L. Stephens (2010), Use of A-Train data to estimate convective buoyancy and entrainment rate, *Geophys. Res. Lett.*, *37*, L09804, doi:10.1029/2010GL042904.

Machado, L. A. T., and W. B. Rossow (1993), Structural characteristics and radiative properties of tropical cloud clusters, *Mon. Weather Rev.*, *121*, 3234–3260, doi:10.1175/1520-0493(1993)121<3234:SCARPO>2.0.CO;2.

Machado, L. A. T., W. B. Rossow, R. L. Guedes, and A. W. Walker (1998), Life cycle variations of mesoscale convective systems over the Americas, *Mon. Weather Rev.*, *126*, 1630–1654.

Petersen, W. A., and S. A. Rutledge (2001), Regional variability in tropical convection: Observations from TRMM, *J. Clim.*, *14*, 3566–3586.

Riehl, H., and J. S. Malkus (1958), On the heat balance in the equatorial trough zone, *Geophysica*, *6*, 503–538.

Riley, E. M., and B. E. Mapes (2009), Unexpected peak near -15°C in CloudSat echo top climatology, *Geophys. Res. Lett.*, *36*, L09819, doi:10.1029/2009GL037558.

Rossow, W. B., and C. Pearl (2007), 22-Year survey of tropical convection penetrating into the lower stratosphere, *Geophys. Res. Lett.*, *34*, L04803, doi:10.1029/2006GL028635.

Shepherd, T. G. (2008), Dynamics, stratospheric ozone, and climate change, *Atmos. Ocean*, *46*, 117–138, doi:10.3137/ao.4601062208.

Sherwood, S. C., and A. E. Dessler (2000), On the control of stratospheric humidity, *Geophys. Res. Lett.*, *27*, 2513–2516.

Soden, B. J., and R. Fu (1995), A satellite analysis of deep convection, upper-tropospheric humidity, and the greenhouse effect, *J. Clim.*, *8*, 2333–2351.

Stephens, G. L., et al. (2008), CloudSat mission: Performance and early science after the first year of operation, *J. Geophys. Res.*, *113*, D00A18, doi:10.1029/2008JD009982.

Su, H., W. G. Read, J. H. Jiang, J. W. Waters, D. L. Wu, and E. J. Fetzer (2006), Enhanced positive water vapor feedback associated with tropical deep convection: New evidence from Aura MLS, *Geophys. Res. Lett.*, *33*, L05709, doi:10.1029/2005GL025505.

Sun, D.-Z., and R. S. Lindzen (1993), Distribution of tropical tropospheric water vapor, *J. Atmos. Sci.*, *50*, 1643–1660.

Takahashi, H., and Z. Luo (2012), Where is the level of neutral buoyancy for deep convection?, *Geophys. Res. Lett.*, *39*, L15809, doi:10.1029/2012GL052638.

Toracinta, E. R., and E. J. Zipser (2001), Lightning and SSM/I-ice-scattering mesoscale convective systems in the global tropics, *J. Appl. Meteorol.*, *40*, 983–1002.

Zipser, E. J. (2003), Some views on "hot towers" after 50 years of tropical field programs and two years of TRMM data, *Meteorol. Monogr.*, *29*, 49–49.

Zipser, E. J., D. J. Cecil, C. Liu, S. W. Nesbitt, and D. P. Yorty (2006), Where are the most intense thunderstorms on Earth?, *Bull. Am. Meteorol. Soc.*, *87*, 1057–1071.